

# Transverse momentum correlations and minijet dissipation in Au-Au collisions at $\sqrt{s_{NN}} = 130$ GeV

J. Adams,<sup>3</sup> M.M. Aggarwal,<sup>29</sup> Z. Ahammed,<sup>43</sup> J. Amonett,<sup>20</sup> B.D. Anderson,<sup>20</sup> D. Arkhipkin,<sup>13</sup> G.S. Averichev,<sup>12</sup> Y. Bai,<sup>27</sup> J. Balewski,<sup>17</sup> O. Barannikova,<sup>32</sup> L.S. Barnby,<sup>3</sup> J. Baudot,<sup>18</sup> S. Bekele,<sup>28</sup> V.V. Belaga,<sup>12</sup> R. Bellwied,<sup>46</sup> J. Berger,<sup>14</sup> B.I. Bezverkhny,<sup>48</sup> S. Bharadwaj,<sup>33</sup> V.S. Bhatia,<sup>29</sup> H. Bichsel,<sup>45</sup> A. Billmeier,<sup>46</sup> L.C. Bland,<sup>4</sup> C.O. Blyth,<sup>3</sup> B.E. Bonner,<sup>34</sup> M. Botje,<sup>27</sup> A. Boucham,<sup>38</sup> A.V. Brandin,<sup>25</sup> A. Bravar,<sup>4</sup> M. Bystersky,<sup>11</sup> R.V. Cadman,<sup>1</sup> X.Z. Cai,<sup>37</sup> H. Caines,<sup>48</sup> M. Calderón de la Barca Sánchez,<sup>4</sup> J. Carroll,<sup>21</sup> J. Castillo,<sup>21</sup> D. Cebra,<sup>7</sup> Z. Chajecki,<sup>44</sup> P. Chaloupka,<sup>11</sup> S. Chattopdhyay,<sup>43</sup> H.F. Chen,<sup>36</sup> Y. Chen,<sup>8</sup> J. Cheng,<sup>41</sup> M. Cherney,<sup>10</sup> A. Chikianian,<sup>48</sup> W. Christie,<sup>4</sup> J.P. Coffin,<sup>18</sup> T.M. Cormier,<sup>46</sup> J.G. Cramer,<sup>45</sup> H.J. Crawford,<sup>6</sup> D. Das,<sup>43</sup> S. Das,<sup>43</sup> M.M. de Moura,<sup>35</sup> A.A. Derevschikov,<sup>31</sup> L. Didenko,<sup>4</sup> T. Dietel,<sup>14</sup> W.J. Dong,<sup>8</sup> X. Dong,<sup>36</sup> J.E. Draper,<sup>7</sup> F. Du,<sup>48</sup> A.K. Dubey,<sup>15</sup> V.B. Dunin,<sup>12</sup> J.C. Dunlop,<sup>4</sup> M.R. Dutta Mazumdar,<sup>43</sup> V. Eckardt,<sup>23</sup> W.R. Edwards,<sup>21</sup> L.G. Efimov,<sup>12</sup> V. Emelianov,<sup>25</sup> J. Engelage,<sup>6</sup> G. Eppley,<sup>34</sup> B. Erazmus,<sup>38</sup> M. Estienne,<sup>38</sup> P. Fachini,<sup>4</sup> J. Faivre,<sup>18</sup> R. Fatemi,<sup>17</sup> J. Fedorisin,<sup>12</sup> K. Filimonov,<sup>21</sup> P. Filip,<sup>11</sup> E. Finch,<sup>48</sup> V. Fine,<sup>4</sup> Y. Fisyak,<sup>4</sup> K.J. Foley,<sup>4</sup> K. Fomenko,<sup>12</sup> J. Fu,<sup>41</sup> C.A. Gagliardi,<sup>39</sup> J. Gans,<sup>48</sup> M.S. Ganti,<sup>43</sup> L. Gaudichet,<sup>38</sup> F. Geurts,<sup>34</sup> V. Ghazikhanian,<sup>8</sup> P. Ghosh,<sup>43</sup> J.E. Gonzalez,<sup>8</sup> O. Grachov,<sup>46</sup> O. Grebenyuk,<sup>27</sup> D. Grosnick,<sup>42</sup> S.M. Guertin,<sup>8</sup> Y. Guo,<sup>46</sup> A. Gupta,<sup>19</sup> T.D. Gutierrez,<sup>7</sup> T.J. Hallman,<sup>4</sup> A. Hamed,<sup>46</sup> D. Hardtke,<sup>21</sup> J.W. Harris,<sup>48</sup> M. Heinz,<sup>2</sup> T.W. Henry,<sup>39</sup> S. Heppelmann,<sup>30</sup> B. Hippolyte,<sup>48</sup> A. Hirsch,<sup>32</sup> E. Hjort,<sup>21</sup> G.W. Hoffmann,<sup>40</sup> H.Z. Huang,<sup>8</sup> S.L. Huang,<sup>36</sup> E.W. Hughes,<sup>5</sup> T.J. Humanic,<sup>28</sup> G. Igo,<sup>8</sup> A. Ishihara,<sup>40</sup> P. Jacobs,<sup>21</sup> W.W. Jacobs,<sup>17</sup> M. Janik,<sup>44</sup> H. Jiang,<sup>8</sup> P.G. Jones,<sup>3</sup> E.G. Judd,<sup>6</sup> S. Kabana,<sup>2</sup> K. Kang,<sup>41</sup> M. Kaplan,<sup>9</sup> D. Keane,<sup>20</sup> V.Yu. Khodyrev,<sup>31</sup> J. Kiryluk,<sup>22</sup> A. Kisiel,<sup>44</sup> E.M. Kislov,<sup>12</sup> J. Klay,<sup>21</sup> S.R. Klein,<sup>21</sup> A. Klyachko,<sup>17</sup> D.D. Koetke,<sup>42</sup> T. Kollegger,<sup>14</sup> M. Kopytine,<sup>20</sup> L. Kotchenda,<sup>25</sup> M. Kramer,<sup>26</sup> P. Kravtsov,<sup>25</sup> V.I. Kravtsov,<sup>31</sup> K. Krueger,<sup>1</sup> C. Kuhn,<sup>18</sup> A.I. Kulikov,<sup>12</sup> A. Kumar,<sup>29</sup> C.L. Kunz,<sup>9</sup> R.Kh. Kutuev,<sup>13</sup> A.A. Kuznetsov,<sup>12</sup> M.A.C. Lamont,<sup>48</sup> J.M. Landgraf,<sup>4</sup> S. Lange,<sup>14</sup> F. Laue,<sup>4</sup> J. Lauret,<sup>4</sup> A. Lebedev,<sup>4</sup> R. Lednický,<sup>12</sup> S. Lehocká,<sup>12</sup> M.J. LeVine,<sup>4</sup> C. Li,<sup>36</sup> Q. Li,<sup>46</sup> Y. Li,<sup>41</sup> S.J. Lindenbaum,<sup>26</sup> M.A. Lisa,<sup>28</sup> F. Liu,<sup>47</sup> L. Liu,<sup>47</sup> Q.J. Liu,<sup>45</sup> Z. Liu,<sup>47</sup> T. Ljubicic,<sup>4</sup> W.J. Llope,<sup>34</sup> H. Long,<sup>8</sup> R.S. Longacre,<sup>4</sup> M. Lopez-Noriega,<sup>28</sup> W.A. Love,<sup>4</sup> Y. Lu,<sup>47</sup> T. Ludlam,<sup>4</sup> D. Lynn,<sup>4</sup> G.L. Ma,<sup>37</sup> J.G. Ma,<sup>8</sup> Y.G. Ma,<sup>37</sup> D. Magestro,<sup>28</sup> S. Mahajan,<sup>19</sup> D.P. Mahapatra,<sup>15</sup> R. Majka,<sup>48</sup> L.K. Mangotra,<sup>19</sup> R. Manweiler,<sup>42</sup> S. Margetis,<sup>20</sup> C. Markert,<sup>48</sup> L. Martin,<sup>38</sup> J.N. Marx,<sup>21</sup> H.S. Matis,<sup>21</sup> Yu.A. Matulenko,<sup>31</sup> C.J. McClain,<sup>1</sup> T.S. McShane,<sup>10</sup> F. Meissner,<sup>21</sup> Yu. Melnick,<sup>31</sup> A. Meschanin,<sup>31</sup> M.L. Miller,<sup>22</sup> Z. Milosevich,<sup>9</sup> N.G. Minaev,<sup>31</sup> C. Mironov,<sup>20</sup> A. Mischke,<sup>27</sup> D. Mishra,<sup>15</sup> J. Mitchell,<sup>34</sup> B. Mohanty,<sup>43</sup> L. Molnar,<sup>32</sup> C.F. Moore,<sup>40</sup> D.A. Morozov,<sup>31</sup> V. Morozov,<sup>21</sup> M.G. Munhoz,<sup>35</sup> B.K. Nandi,<sup>43</sup> T.K. Nayak,<sup>43</sup> J.M. Nelson,<sup>3</sup> P.K. Netrakanti,<sup>43</sup> V.A. Nikitin,<sup>13</sup> L.V. Nogach,<sup>31</sup> B. Norman,<sup>20</sup> S.B. Nurushev,<sup>31</sup> G. Odyniec,<sup>21</sup> A. Ogawa,<sup>4</sup> V. Okorokov,<sup>25</sup> M. Oldenburg,<sup>21</sup> D. Olson,<sup>21</sup> S.K. Pal,<sup>43</sup> Y. Panebratsev,<sup>12</sup> S.Y. Panitkin,<sup>4</sup> A.I. Pavlinov,<sup>46</sup> T. Pawlak,<sup>44</sup> T. Peitzmann,<sup>27</sup> V. Perevozchikov,<sup>4</sup> C. Perkins,<sup>6</sup> W. Peryt,<sup>44</sup> V.A. Petrov,<sup>13</sup> S.C. Phatak,<sup>15</sup> R. Picha,<sup>7</sup> M. Planinic,<sup>49</sup> J. Pluta,<sup>44</sup> N. Porile,<sup>32</sup> J. Porter,<sup>45</sup> A.M. Poskanzer,<sup>21</sup> M. Potekhin,<sup>4</sup> E. Potrebenikova,<sup>12</sup> B.V.K.S. Potukuchi,<sup>19</sup> D. Prindle,<sup>45</sup> C. Pruneau,<sup>46</sup> J. Putschke,<sup>23</sup> G. Rai,<sup>21</sup> G. Rakness,<sup>30</sup> R. Raniwala,<sup>33</sup> S. Raniwala,<sup>33</sup> O. Ravel,<sup>38</sup> R.L. Ray,<sup>40</sup> S.V. Razin,<sup>12</sup> D. Reichhold,<sup>32</sup> J.G. Reid,<sup>45</sup> G. Renault,<sup>38</sup> F. Retiere,<sup>21</sup> A. Ridiger,<sup>25</sup> H.G. Ritter,<sup>21</sup> J.B. Roberts,<sup>34</sup> O.V. Rogachevskiy,<sup>12</sup> J.L. Romero,<sup>7</sup> A. Rose,<sup>46</sup> C. Roy,<sup>38</sup> L. Ruan,<sup>36</sup> I. Sakrejda,<sup>21</sup> S. Salur,<sup>48</sup> J. Sandweiss,<sup>48</sup> I. Savin,<sup>13</sup> P.S. Sazhin,<sup>12</sup> J. Schambach,<sup>40</sup> R.P. Scharenberg,<sup>32</sup> N. Schmitz,<sup>23</sup> L.S. Schroeder,<sup>21</sup> K. Schweda,<sup>21</sup> J. Seger,<sup>10</sup> P. Seyboth,<sup>23</sup> E. Shahaliev,<sup>12</sup> M. Shao,<sup>36</sup> W. Shao,<sup>5</sup> M. Sharma,<sup>29</sup> W.Q. Shen,<sup>37</sup> K.E. Shesternov,<sup>31</sup> S.S. Shimanskiy,<sup>12</sup> F. Simon,<sup>23</sup> R.N. Singaraju,<sup>43</sup> G. Skoro,<sup>12</sup> N. Smirnov,<sup>48</sup> R. Snellings,<sup>27</sup> G. Sood,<sup>42</sup> P. Sorensen,<sup>21</sup> J. Sowinski,<sup>17</sup> J. Speltz,<sup>18</sup> H.M. Spinka,<sup>1</sup> B. Srivastava,<sup>32</sup> A. Stadnik,<sup>12</sup> T.D.S. Stanislaus,<sup>42</sup> R. Stock,<sup>14</sup> A. Stolpovsky,<sup>46</sup> M. Strikhanov,<sup>25</sup> B. Stringfellow,<sup>32</sup> A.A.P. Suade,<sup>35</sup> E. Sugarbaker,<sup>28</sup> C. Suire,<sup>4</sup> M. Sumbera,<sup>11</sup> B. Surrow,<sup>22</sup> T.J.M. Symons,<sup>21</sup> A. Szanto de Toledo,<sup>35</sup> P. Szarwas,<sup>44</sup> A. Tai,<sup>8</sup> J. Takahashi,<sup>35</sup> A.H. Tang,<sup>27</sup> T. Tarnowsky,<sup>32</sup> D. Thein,<sup>8</sup> J.H. Thomas,<sup>21</sup> S. Timoshenko,<sup>25</sup> M. Tokarev,<sup>12</sup> T.A. Trainor,<sup>45</sup> S. Trentalange,<sup>8</sup> R.E. Tribble,<sup>39</sup> O.D. Tsai,<sup>8</sup> J. Ulery,<sup>32</sup> T. Ullrich,<sup>4</sup> D.G. Underwood,<sup>1</sup> A. Urkinbaev,<sup>12</sup> G. Van Buren,<sup>4</sup> M. van Leeuwen,<sup>21</sup> A.M. Vander Molen,<sup>24</sup> R. Varma,<sup>16</sup> I.M. Vasilevski,<sup>13</sup> A.N. Vasiliev,<sup>31</sup> R. Vernet,<sup>18</sup> S.E. Vigdor,<sup>17</sup> V.P. Viyogi,<sup>43</sup> S. Vokal,<sup>12</sup> S.A. Voloshin,<sup>46</sup> M. Vznuzdaev,<sup>25</sup> W.T. Waggoner,<sup>10</sup> F. Wang,<sup>32</sup> G. Wang,<sup>20</sup> G. Wang,<sup>5</sup> X.L. Wang,<sup>36</sup> Y. Wang,<sup>40</sup> Y. Wang,<sup>41</sup> Z.M. Wang,<sup>36</sup> H. Ward,<sup>40</sup> J.W. Watson,<sup>20</sup> J.C. Webb,<sup>17</sup> R. Wells,<sup>28</sup> G.D. Westfall,<sup>24</sup> A. Wetzler,<sup>21</sup> C. Whitten Jr.,<sup>8</sup> H. Wieman,<sup>21</sup> S.W. Wissink,<sup>17</sup> R. Witt,<sup>2</sup> J. Wood,<sup>8</sup> J. Wu,<sup>36</sup> N. Xu,<sup>21</sup> Z. Xu,<sup>4</sup> Z.Z. Xu,<sup>36</sup> E. Yamamoto,<sup>21</sup> P. Yepes,<sup>34</sup> V.I. Yurevich,<sup>12</sup> Y.V. Zanevsky,<sup>12</sup> H. Zhang,<sup>4</sup> W.M. Zhang,<sup>20</sup> Z.P. Zhang,<sup>36</sup> P.A. Zolnierczuk,<sup>17</sup> R. Zoukarneev,<sup>13</sup> Y. Zoukarneeva,<sup>13</sup> and A.N. Zubarev<sup>12</sup>

(STAR Collaboration)

<sup>1</sup>*Argonne National Laboratory, Argonne, Illinois 60439*  
<sup>2</sup>*University of Bern, 3012 Bern, Switzerland*  
<sup>3</sup>*University of Birmingham, Birmingham, United Kingdom*  
<sup>4</sup>*Brookhaven National Laboratory, Upton, New York 11973*  
<sup>5</sup>*California Institute of Technology, Pasadena, California 91125*  
<sup>6</sup>*University of California, Berkeley, California 94720*  
<sup>7</sup>*University of California, Davis, California 95616*  
<sup>8</sup>*University of California, Los Angeles, California 90095*  
<sup>9</sup>*Carnegie Mellon University, Pittsburgh, Pennsylvania 15213*  
<sup>10</sup>*Creighton University, Omaha, Nebraska 68178*  
<sup>11</sup>*Nuclear Physics Institute AS CR, 250 68 Řež/Prague, Czech Republic*  
<sup>12</sup>*Laboratory for High Energy (JINR), Dubna, Russia*  
<sup>13</sup>*Particle Physics Laboratory (JINR), Dubna, Russia*  
<sup>14</sup>*University of Frankfurt, Frankfurt, Germany*  
<sup>15</sup>*Institute of Physics, Bhubaneswar 751005, India*  
<sup>16</sup>*Indian Institute of Technology, Mumbai, India*  
<sup>17</sup>*Indiana University, Bloomington, Indiana 47408*  
<sup>18</sup>*Institut de Recherches Subatomiques, Strasbourg, France*  
<sup>19</sup>*University of Jammu, Jammu 180001, India*  
<sup>20</sup>*Kent State University, Kent, Ohio 44242*  
<sup>21</sup>*Lawrence Berkeley National Laboratory, Berkeley, California 94720*  
<sup>22</sup>*Massachusetts Institute of Technology, Cambridge, MA 02139-4307*  
<sup>23</sup>*Max-Planck-Institut für Physik, Munich, Germany*  
<sup>24</sup>*Michigan State University, East Lansing, Michigan 48824*  
<sup>25</sup>*Moscow Engineering Physics Institute, Moscow Russia*  
<sup>26</sup>*City College of New York, New York City, New York 10031*  
<sup>27</sup>*NIKHEF, Amsterdam, The Netherlands*  
<sup>28</sup>*Ohio State University, Columbus, Ohio 43210*  
<sup>29</sup>*Panjab University, Chandigarh 160014, India*  
<sup>30</sup>*Pennsylvania State University, University Park, Pennsylvania 16802*  
<sup>31</sup>*Institute of High Energy Physics, Protvino, Russia*  
<sup>32</sup>*Purdue University, West Lafayette, Indiana 47907*  
<sup>33</sup>*University of Rajasthan, Jaipur 302004, India*  
<sup>34</sup>*Rice University, Houston, Texas 77251*  
<sup>35</sup>*Universidade de São Paulo, São Paulo, Brazil*  
<sup>36</sup>*University of Science & Technology of China, Anhui 230027, China*  
<sup>37</sup>*Shanghai Institute of Applied Physics, Shanghai 201800, China*  
<sup>38</sup>*SUBATECH, Nantes, France*  
<sup>39</sup>*Texas A&M University, College Station, Texas 77843*  
<sup>40</sup>*University of Texas, Austin, Texas 78712*  
<sup>41</sup>*Tsinghua University, Beijing 100084, China*  
<sup>42</sup>*Valparaiso University, Valparaiso, Indiana 46383*  
<sup>43</sup>*Variable Energy Cyclotron Centre, Kolkata 700064, India*  
<sup>44</sup>*Warsaw University of Technology, Warsaw, Poland*  
<sup>45</sup>*University of Washington, Seattle, Washington 98195*  
<sup>46</sup>*Wayne State University, Detroit, Michigan 48201*  
<sup>47</sup>*Institute of Particle Physics, CCNU (HZNU), Wuhan 430079, China*  
<sup>48</sup>*Yale University, New Haven, Connecticut 06520*  
<sup>49</sup>*University of Zagreb, Zagreb, HR-10002, Croatia*

(Dated: May 23, 2019)

We present the first measurements of two-particle correlations on transverse momentum  $p_t$  for Au-Au collisions at  $\sqrt{s_{NN}} = 130$  GeV. Significant large-momentum-scale correlation structures are observed for charged primary hadrons with  $0.15 \leq p_t \leq 2$  GeV/c and pseudorapidity  $|\eta| \leq 1.3$ . Such correlations were not observed in a similar study at lower energy and are not predicted by theoretical collision models. The observed correlation structure is consistent with a scenario in which initial-state semi-hard parton scattering and fragmentation are modified by in-medium dissipation.

PACS numbers: 24.60.-k, 24.60.Ky, 25.75.-q, 25.75.Gz

Two-particle correlations and associated nonstatistical fluctuations in relativistic heavy ion collisions probe the dynamics of parton scattering and nonperturbative as-

pects of quantum chromodynamics [1, 2, 3]. Substantial nonstatistical fluctuations in the event-wise mean transverse momentum  $\langle p_t \rangle$  of charged particles from Au-

Au collisions have been reported by the STAR [4] and PHENIX [5] experiments at the Relativistic Heavy Ion Collider (RHIC).  $\langle p_t \rangle$  fluctuations at RHIC are much larger than those reported at the CERN Super Proton Synchrotron (SPS) with one-tenth the CM energy [6], and were not predicted by theoretical models [4, 7, 8]. Such fluctuations could result from incompletely equilibrated initial-state multiple scattering (ISS) [9] or minijet production [7], the increased hard-scattering cross section at RHIC energies producing greater two-particle correlations there. In this Letter we report the first study of the dynamical origins of  $\langle p_t \rangle$  fluctuations using two-particle correlations on transverse momentum  $p_t$  in Au-Au collisions at  $\sqrt{s_{NN}} = 130$  GeV (CM energy per nucleon-nucleon pair) observed with the STAR detector at RHIC.

Nonstatistical event-wise  $\langle p_t \rangle$  fluctuations, measured as a variance excess by quantity  $\Delta\sigma_{p_t:n}^{2(CI)}$  introduced in [4], can be expressed as a  $p_t$ -weighted integral of two-particle correlations measured by a pair-ratio distribution.  $\Delta\sigma_{p_t:n}^{2(CI)}$  can be rewritten in terms of discrete sums over  $p_t$  products [10], in turn approximated by a weighted integral of the difference between pair-number densities for correlated (same-event, sibling) pairs  $\rho_{sib}(p_{t1}, p_{t2})$  and uncorrelated (mixed-event) pairs  $\rho_{mix}(p_{t1}, p_{t2})$ , as

$$\begin{aligned} \Delta\sigma_{p_t:n}^{2(CI)} &\equiv \frac{1}{\varepsilon} \sum_{j=1}^{\varepsilon} \left\{ \frac{1}{n_j} \sum_{i \neq i'=1}^{n_j} (p_{tji} p_{tji'} - \hat{p}_t^2) \right\} \quad (1) \\ &= \frac{1}{\bar{N}} \int \int dp_{t1} dp_{t2} p_{t1} p_{t2} (\rho_{sib} - \rho_{mix}) \\ &= (\bar{N} - 1) \hat{p}_t^2 \langle r(p_{t1}, p_{t2}) - 1 \rangle, \end{aligned}$$

where pair ratio  $r \equiv \rho_{sib}/\rho_{mix}$  is introduced in the last line. Superscript CI (charge independent) indicates that the sums include all charges,  $\varepsilon$  is the number of events in a centrality bin,  $j$  is the event index,  $n_j$  is the number of accepted particles in event  $j$ ,  $\hat{p}_t$  is the mean of the inclusive  $p_t$  distribution (all accepted particles from all events in a centrality bin),  $i$  and  $i'$  are particle indices and  $\bar{N}$  is the mean event multiplicity in the acceptance. The angle brackets denote a normalized expectation value with weight  $p_{t1} p_{t2} \rho_{mix}(p_{t1}, p_{t2})$ . In this paper we present two-particle  $p_t$  correlations measured by pair-ratio distribution  $r(p_{t1}, p_{t2})$  corresponding to excess  $\langle p_t \rangle$  fluctuations.

Data were obtained with the STAR Time Projection Chamber (TPC) [11]. Triggering, tracking details, quality cuts and primary-particle definition are discussed in [4]. The data consisted of 300k events divided into four centrality classes [12] defined by cuts on TPC track multiplicity  $N$  within  $|\eta| \leq 1.3$ ,  $0.15 \leq p_t \leq 2$  GeV/ $c$ , and full azimuthal acceptance. Densities  $\rho_{sib}$  and  $\rho_{mix}$  were approximated respectively by symmetrized pair-number histograms  $n_{kl,sib}$  and  $n_{kl,mix}$ . Particle pairs for each charge-sign combination were summed into two-dimensional bins ( $kl$ ) on  $(p_{t1}, p_{t2})$ . Density ratios  $r$  for four charge combinations ( $a=\pm, b=\pm$ ) were approximated by normalized ratio histograms  $\hat{r}_{ab,kl} \equiv \hat{n}_{ab,kl,sib}/\hat{n}_{ab,kl,mix}$ , with  $\hat{n}_{ab,kl} = n_{ab,kl}/\sum_{kl} n_{ab,kl}$ . Corrections

were made to  $\hat{r}_{kl}$  for two-track inefficiencies caused by overlapping space points in the TPC and intersecting trajectories reconstructed as  $> 2$  particles [13]. Mixed pairs were formed from event pairs with multiplicities differing by  $\leq 100$  ( $N \sim 10^3$  for central collisions) and primary-vertex axial positions differing by  $\leq 7.5$  cm [14]. Four charge-sign combinations were summed as like-sign (LS), unlike-sign (US), and charge-independent (CI=LS+US).

Measured LS and US normalized pair ratios  $\hat{r}_{kl}$  for most-central collisions are shown in Fig. 1. Data were binned linearly on quantity  $X(p_t) \equiv 1 - \exp\{-(m_t - m_\pi)/0.4\}$  GeV  $\in [0, 1]$  ( $m_t = \sqrt{p_t^2 + m_\pi^2}$ , pion mass  $m_\pi$  assumed) with bin size 1/25 to achieve approximately uniform statistical accuracy over the binned acceptance. The small-momentum-scale correlations (low- $X(p_t)$  peaks) are attributed to quantum correlations (HBT) and Coulomb interactions based on MC simulations [15, 16]. The dominant features are a large-momentum-scale correlation (LSC) ‘saddle’ structure with positive (negative) curvature along the  $X(p_t)_{\Sigma(\Delta)} \equiv X(p_{t1}) + (-) X(p_{t2})$  sum (difference) direction and a narrow peak structure at large  $X(p_t)$  ( $p_t > 0.6$  GeV/ $c$ ).

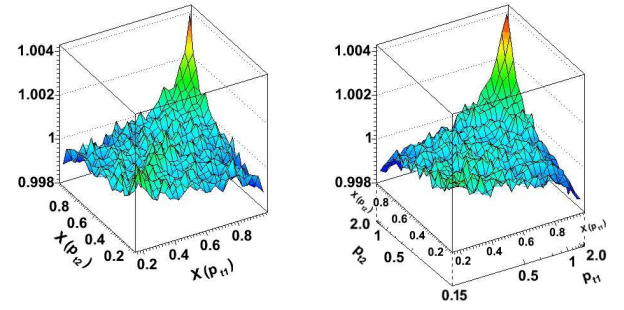


FIG. 1: Symmetrized pair-density ratios  $\hat{r}_{kl}$  on  $X(p_{t1})$  vs  $X(p_{t2})$  for like-sign (left panel) and unlike-sign (right panel) unidentified charged primary particles for most-central Au-Au collision events. Note auxiliary  $p_t$  scale in units GeV/ $c$ .

Centrality dependence of LSC structures is shown in Fig. 2 for CI net pair-ratio combination ( $\hat{r}_{kl} - 1$ ). HBT and Coulomb correlations are removed here by discarding sibling and mixed pairs with  $|\eta_1 - \eta_2| < 0.3$ ,  $|\phi_1 - \phi_2| < \pi/6$  (azimuth),  $|p_{t1} - p_{t2}| < 0.15$  GeV/ $c$ , if  $p_t < 0.8$  GeV/ $c$  for either particle. With increasing centrality the negative saddle curvature along the difference increases in magnitude, the positive curvature along the sum decreases, and the magnitude of the peak at large  $X(p_t)$  also decreases. A similar analysis of Pb-Pb collisions by experiment NA49 at the CERN SPS observed no significant CI correlations for  $1.1 < y_{cm} < 2.6$  [17].

Per-bin statistical errors for  $\hat{r}_{kl} - 1$  in Fig. 2 are  $\sim 15\%$  of maximum correlation amplitude for each centrality. Systematic errors, estimated as in [4], include tracking errors from the TPC central membrane but are dominated by contamination from non-primary background particles, mainly weak-decay daughters [18]. Correlation contributions from the latter were assumed to vary

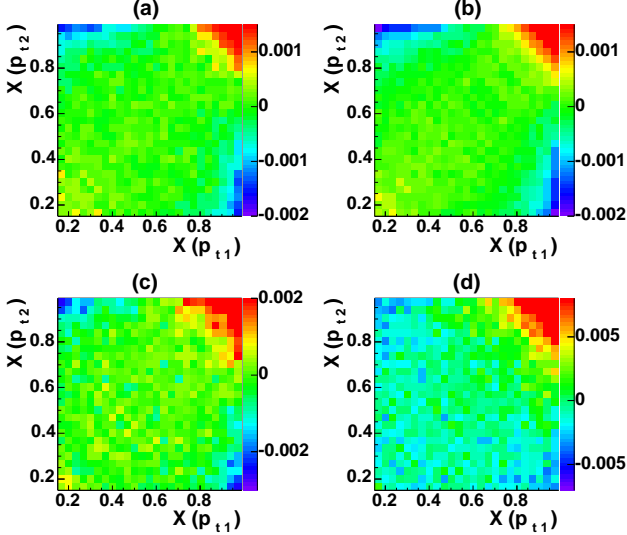


FIG. 2: Pair-density net ratios  $r[X(p_{t1}), X(p_{t2})] - 1$  for all nonidentified charged primary particles for (a) most-central, (b) mid-central, (c) mid-peripheral, and (d) peripheral Au-Au collision events. Note scale change for panels (c) and (d).

from zero to the same correlation amplitude as the primary particles. Multiplicative corrections (not applied to data in Figs. 1 and 2) and total systematic errors for  $\hat{r}_{kl} - 1$  were obtained from the average and half difference respectively of the limiting cases and varied from 1.07 and  $\pm 7\%$  for  $X(p_{t1,2}) > 0.4$  up to 1.16 and  $\pm 16\%$  for  $X(p_{t1,2}) < 0.4$  and 1.12 and  $\pm 12\%$  in the off-diagonal corners. Resonance decays ( $\rho^0, \omega$ ) were estimated via simulations [16] to contribute a small saddle-shape correlation with amplitude  $\sim 0.0002(\bar{N}_{\text{most-central}}/\bar{N})$  at the corners of Fig. 1 and each panel of Fig. 2, and curvature opposite to data.

The principal features in Fig. 2 can be described by two physically-motivated correlation models, the first (saddle) describing local temperature and/or collective velocity fluctuations on  $(\eta, \phi)$ , the second (large- $X(p_t)$  peak) representing semi-hard scattering correlations and determined from p-p collisions at RHIC [19]. An equilibrated system is described by global temperature parameter  $\beta_0 \equiv 1/T_0$ . If the system is incompletely equilibrated the local velocity/temperature distribution at hadronization can be represented by event-wise varying distribution  $\beta(\eta, \phi)$ . This distribution determines the shapes of the effective *local-parent*  $p_t$  spectra  $\exp\{-\beta(\eta, \phi)(m_t - m_\pi)\}$  sampled in each event by final-state hadrons. Fluctuations in quantity  $\beta$  linearly represent fluctuations in  $1/T$  and/or  $v/c$  of the local-parent  $p_t$  spectra. If the distribution of  $\beta(\eta, \phi)$  values over an event ensemble is represented by  $g_1(\beta)$ , with centroid  $\beta_0$  and variance  $\sigma_\beta^2$ , the inclusive single-particle  $p_t$  spectrum is determined by convoluting thermal spectrum  $e^{-\beta(m_t - m_\pi)}$  with  $g_1(\beta)$ . If  $g_1(\beta)$  is modeled by a gamma distribution [20] then  $1/p_t dN/dp_t = A/\{1 + \beta_0(m_t - m_\pi)/n\}^n$ , a Lévy dis-

tribution [21] with exponent  $1/n = \sigma_\beta^2/\beta_0^2$ , the *relative variance* of  $g_1(\beta)$ .

By a similar argument hadron pairs sample local-parent two-particle  $p_t$  spectra with shapes determined by two-dimensional (2D) temperature/velocity distribution  $g_2(\beta_1, \beta_2)$ . For uncorrelated  $\beta$  fluctuations or mixed pairs (particles from different events) this distribution factorizes,  $g_2(\beta_1, \beta_2) = g_1(\beta_1) \cdot g_1(\beta_2)$ , and therefore has zero covariance. For *global* fluctuations (event-wise-uniform  $\beta$  varying between events)  $g_2(\beta_1, \beta_2) \propto g'_1(\beta_1)\delta(\beta_1 - \beta_2)$ , a diagonal locus with maximum covariance. The inclusive two-particle  $(p_{t1}, p_{t2})$  spectrum is the convolution of thermal spectrum  $e^{-\beta_1(m_{t1} - m_\pi)}e^{-\beta_2(m_{t2} - m_\pi)}$  with  $g_2(\beta_1, \beta_2)$ . If  $g_2(\beta_1, \beta_2)$  is modelled by a 2D gamma distribution with arbitrary nonzero covariance the two-particle  $(p_{t1}, p_{t2})$  spectrum is well approximated by 2D Lévy model distribution

$$F_{sib} \propto \left(1 + \frac{\beta_0 m_{t\Sigma}}{2n_\Sigma}\right)^{-2n_\Sigma} \left[1 - \left(\frac{\beta_0 m_{t\Delta}}{2n_\Delta + \beta_0 m_{t\Sigma}}\right)^2\right]^{-n_\Delta} \quad (2)$$

on sum and difference variables  $m_{t\Sigma} \equiv m_{t1} + m_{t2} - 2m_\pi$  and  $m_{t\Delta} \equiv m_{t1} - m_{t2}$ .  $1/n_\Sigma$  and  $1/n_\Delta$  are the relative variances of  $g_2(\beta_1, \beta_2)$  along sum and difference variables  $\beta_\Sigma$  and  $\beta_\Delta$  respectively, and  $\Delta(1/n)_{tot} \equiv 1/n_\Sigma - 1/n_\Delta$  is the relative *covariance* [22] which measures velocity/temperature correlations. Mixed-pair distribution  $F_{mix}(p_{t1}, p_{t2})$ , modeled by the product of single-particle Lévy distributions, has the same form as Eq. (2) but with  $n_\Sigma = n_\Delta = n$  ( $g_2$  then has zero covariance). Ratio  $r_{model} \equiv F_{sib}/F_{mix}$  was fitted to data in Fig. 2. Relative variance *differences*  $\Delta(1/n)_\Sigma \equiv (1/n_\Sigma - 1/n)$  and  $\Delta(1/n)_\Delta \equiv (1/n_\Delta - 1/n)$  measure the curvatures of histogram  $\hat{r}_{kl}$  along sum and difference axes near the origin.

Data in Fig. 2 (excluding peak region  $X(p_t)_\Sigma > 1.6$ ) were fitted with  $r_{model} - 1 + \mathcal{C}$  by varying parameters  $n_\Sigma$ ,  $n_\Delta$  and  $\mathcal{C}$  (offset). Parameter  $\beta_0 = 5 \text{ GeV}^{-1}$  is fixed by the inclusive single-particle  $p_t$  distribution for  $p_t < 1 \text{ GeV}/c$ . Parameter  $1/n \equiv 1/n_{flow} + 1/n_{fluct}$ , also derived from the 1D  $p_t$  distribution, represents a combination of transverse expansion (radial flow) and the velocity/temperature fluctuations (including hard scattering) assumed above. Since the component  $1/n_{fluct}$  relevant to the Lévy saddle fit is not directly accessible, fits to 2D  $\hat{r} - 1$  distributions only weakly constrain absolute quantities  $1/n_\Sigma$  and  $1/n_\Delta$ . However, corresponding *differences*  $\Delta(1/n)_{\Sigma, \Delta}$  are well determined by the saddle curvatures nearly independently of  $1/n_{fluct}$ . A value  $1/n_{fluct} = 0.03$  near the center of the allowed range  $1/13$  [18] to 0.0012 (Table I) was chosen to insure stable  $\Delta(1/n)_\Sigma$  and  $\Delta(1/n)_\Delta$  fit values. If  $1/n_{fluct}$  were actually measured, comparison of  $g_2$  covariance to  $g_1$  variance *via* linear correlation coefficient  $\kappa \equiv (1/n_\Sigma - 1/n_\Delta)/(1/n_\Sigma + 1/n_\Delta) \simeq \Delta(1/n)_{tot}/(2/n_{fluct})$  (assumes  $n_\Sigma \sim n_\Delta \sim n_{fluct}$ ) would determine whether velocity/temperature fluctuations are nearly uncorrelated ( $\kappa \sim 0$ ) or nearly global ( $\kappa \sim 1$ ). Best-fit parameters and  $\chi^2/\text{DoF}$  for the saddle fits are listed in Table I. The model function and residuals for

the fit to centrality (b) are shown in Fig. 3.

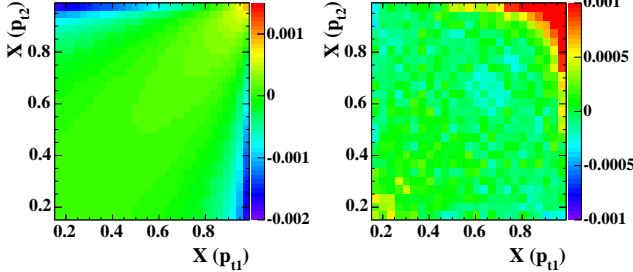


FIG. 3: Left: pair-density net ratio  $r[X(p_{t1}), X(p_{t2})] - 1$  for model fit to mid-central (b) Au-Au collisions. Right: residuals (data – model) for mid-central collisions (note scale change).

Two-dimensional saddle-fit residuals, as in Fig. 3, are independent of difference  $X(p_t)_\Delta = X(p_{t1}) - X(p_{t2})$ , indicating that the Lévy temperature fluctuation model adequately describes the saddle structure. Residuals from the 2D saddle fit for mid-central events (b) are shown in Fig. 4 (left panel) projected onto sum variable  $X(p_t)_\Sigma$ . Residuals for other centralities are similar in form but differ in amplitude. We speculate that this residual structure is due to semi-hard parton scattering (minijets) [19].

The last row in Table I lists the multiplicity extrapolation factor  $\mathcal{S}$  for contamination and tracking inefficiency from [4]. Centrality dependence on mean participant path length  $\nu$  [23] of those model parameters which determine saddle amplitudes in Fig. 2 are shown in Fig. 4 (right panel). Multiplication by  $\mathcal{S}\bar{N}$  estimates the correlation amplitude per final-state hadron [24]. The linear trends are notable.

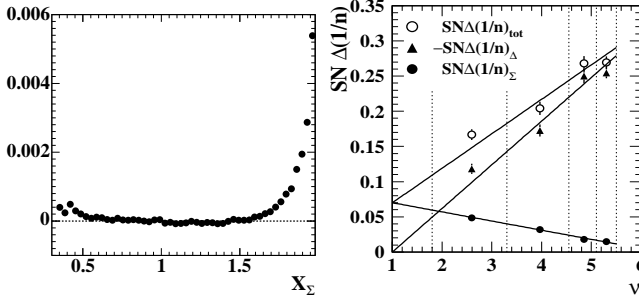


FIG. 4: Left: Residuals from 2D Lévy saddle fit to mid-central (b) data in Fig. 2 projected onto sum variable  $X(p_t)_\Sigma$ . Right: Saddle curvature measures on centrality, with extrapolation factor  $\mathcal{S}$  and multiplicity  $\bar{N}$  [24]:  $\mathcal{S}\bar{N}\Delta(1/n)_\Sigma$  (dots),  $-\mathcal{S}\bar{N}\Delta(1/n)_\Delta$  (triangles) and  $\mathcal{S}\bar{N}\Delta(1/n)_{tot}$  (open circles). Linear trends on mean participant path length  $\nu$  [23] are shown. Data symbols include fitting errors only. Systematic errors (not shown) range from 11-14% [25].

If  $\sigma_\beta^2$  were dominated by temperature fluctuations ( $\beta \rightarrow 1/T$ ), this fixed-scale (full-acceptance) correlation measurement of saddle curvatures would set a *lower* limit on local temperature fluctuations (or *upper* limit on global fluctuations)  $\sigma_\beta/\beta_0 \rightarrow \sigma_T/T_0 \geq \sqrt{\Delta(1/n)_{tot}/2} \sim$

TABLE I: Parameters and fitting errors (only) for 2D velocity/temperature fluctuation model for each centrality bin, (a) - (d) (*i.e.*, central - peripheral as in Fig. 2). Errors (last column) represent the range in fitting uncertainties. Systematic errors range over 7-12% [25]. Extrapolation factors  $\mathcal{S}$  are listed in the last row [24].

centrality	(d)	(c)	(b)	(a)	error <sup>a</sup> (%)
$N$	115.5	424.9	790.2	983.0	
$\mathcal{C} \times 10^4$	-11.6	-0.820	0.787	0.750	6-14
$\Delta(1/n)_\Sigma \times 10^4$	3.54	0.611	0.183	0.118	6-24
$\Delta(1/n)_\Delta \times 10^4$	-8.61	-3.33	-2.53	-2.04	6-3
$\Delta(1/n)_{tot} \times 10^4$	12.2	3.95	2.71	2.16	
$\chi^2/\text{DoF}$	$\frac{348}{286}$	$\frac{313}{286}$	$\frac{475}{286}$	$\frac{402}{286}$	
$\mathcal{S}$	1.19	1.22	1.25	1.27	$8^b$

<sup>a</sup>Range of fitting errors in percent from peripheral to central.

<sup>b</sup>Systematic error.

1% for central events. Upper limit  $\sigma_T/T_0 \leq \sqrt{1/n} \sim 30\%$  on local fluctuations is derived from the inclusive  $p_t$  distribution. Local  $\beta$  fluctuations are studied in more detail *via* direct measurement of  $p_t$  correlations on  $(\eta, \phi)$ .

We further interpret the overall correlation structure in Fig. 2 in terms of in-medium modification of a two-particle fragmentation function on  $(p_{t1}, p_{t2})$ . Minijet production in A-A collisions should increase linearly with mean path length  $\nu$  [23]. That expectation is consistent with observed linear increase of total curvature  $\mathcal{S}\bar{N}\Delta(1/n)_{tot}$  (increasing  $g_2$  covariance) in Fig. 4. We also observe in Fig. 4 a) reduced curvature along the sum direction and b) increased curvature along the difference direction which may represent respectively transport of semi-hard parton structure to lower  $p_t$  and a more correlated prehadronic bulk medium. Given the minijet interpretation of  $\mathcal{S}\bar{N}\Delta(1/n)_{tot}$ , combined trends a) and b) represent striking evidence for increased parton dissipation in the more central Au-Au collisions and may be compared to the observed suppression of  $R_{AA}$  in central Au-Au collisions at RHIC [26].

HJING [7], which models color-string fragmentation and minijets, exhibits excessive correlation structure at low and high  $p_t$  ( $X(p_t)_\Sigma < 0.5$  and  $> 1.6$ , respectively) compared to data, displaying a saddle shape which is qualitatively different from the 2D Lévy model and data. RQMD [8], which models a resonance gas, predicts a saddle-shape distribution as well, but with amplitude and form also qualitatively different from the 2D Lévy model and data. Fit *residuals* for HJING and RQMD relative to Lévy saddle fits are highly structured, and up to several times the corresponding *amplitudes* of saddle fits to data.

The dynamical origins of excess  $\langle p_t \rangle$  fluctuations [4, 5] in Au-Au collisions at RHIC are probed in this first analysis of  $p_{t1}$  vs  $p_{t2}$  correlations. The velocity/temperature structure of heavy ion collisions inferred from those correlations is unanticipated by theoretical models. The observed correlations on  $p_t$  may be interpreted as resulting from semi-hard parton scattering and subsequent fragmentation (minijets) in which partons are strongly mod-

ified by in-medium dissipation in the more central Au-Au collisions. In this picture, with increasing centrality the two-particle fragmentation function is shifted to lower  $p_t$  and asymptotically approaches a form consistent with a structured velocity/temperature distribution (Lévy saddle) as part of an incomplete equilibration process. These newly observed  $p_t$  correlations may thus reveal dissipative modification of the two-particle parton fragmentation function in the medium produced by Au-Au collisions at RHIC. Followup studies of  $p_t$  correlation structure on  $(\eta, \phi)$  should further clarify this picture.

We thank the RHIC Operations Group and RCF at

BNL, and the NERSC Center at LBNL for their support. This work was supported in part by the HENP Divisions of the Office of Science of the U.S. DOE; the U.S. NSF; the BMBF of Germany; IN2P3, RA, RPL, and EMN of France; EPSRC of the United Kingdom; FAPESP of Brazil; the Russian Ministry of Science and Technology; the Ministry of Education and the NNSFC of China; Grant Agency of the Czech Republic, FOM and UU of the Netherlands, DAE, DST, and CSIR of the Government of India; Swiss NSF; and the Polish State Committee for Scientific Research.

---

[1] R. Stock, Nucl. Phys. **A661**, 282 (1999); H. Heiselberg, Phys. Rep. **351**, 161 (2001).

[2] M. Stephanov, K. Rajagopal, E. Shuryak, Phys. Rev. D **60**, 114028 (1999).

[3] A. Dumitru, R. Pisarski, Phys. Lett. **B504**, 282 (2001).

[4] J. Adams *et al.* (STAR Collaboration), nucl-ex/0308033.

[5] S. S. Adler *et al.* (PHENIX Collaboration), nucl-ex/0310005.

[6] H. Appelshäuser *et al.* (NA49 Collaboration), Phys. Lett. **B459**, 679 (1999); D. Adamová *et al.*, (CERES Collaboration), Nucl. Phys. **A727**, 97 (2003).

[7] X.N. Wang, M. Gyulassy, Phys. Rev. D **44**, 3501 (1991).

[8] H. Sorge, H. Stöcker, W. Greiner, Nucl. Phys. **A498**, 567c (1989); Ann. Phys. (N.Y.) **192**, 266 (1989).

[9] M. Gaździcki, A. Leonidov, G. Roland, Eur. Phys. J. **C6**, 365 (1999).

[10] T. A. Trainor, eprint hep-ph/0001148, unpublished.

[11] K. H. Ackermann *et al.*, Nucl. Instrum. Meth. A **499**, 624 (2003); see other STAR papers in volume **A499**.

[12] Four centrality classes were defined by  $N/N_0$  cuts at  $> 0.029$ ,  $0.21$ ,  $0.56$  and  $> 0.79$  corresponding to fraction of total cross section bounds:  $> 0.7$ ,  $0.4$ ,  $0.17$  and  $> 0.05$ .  $N_0$  is the half-maximum point at the end of the minimum-bias distribution plotted as  $d\sigma/dN^{1/4}$ , and is an estimator on  $N$  for the maximum number of participants, where  $N_{part}/N_{part,max} \simeq N/N_0$  within 4%.

[13] Track-pair cuts required  $\geq 10$  cm average track separation for nine radial positions in the TPC. Crossing tracks with separations at the TPC mid-radius  $< 10$  cm (beam direction) and  $< 30$  cm (azimuth) were removed.

[14] J. G. Reid and T. A. Trainor, Nucl. Instrum. Meth. A **457**, 378-383 (2001).

[15] C. Adler *et al.* Phys. Rev. Lett. **87**, 082301 (2001).

[16] R. Ray and R. Longacre, nucl-ex/0008009, unpublished.

[17] J. G. Reid, Ph. D. thesis, Univ. of Washington, nucl-ex/0302001.

[18] Related to but not equivalent to the power-law exponent in C. Adler *et al.*, Phys. Rev. Lett. **87**, 112303 (2001); *ibid.* **89**, 202301 (2002).

[19] R. J. Porter and T. A. Trainor (STAR Collaboration), hep-ph/0406330.

[20] M.J. Tannenbaum, Phys. Lett. **B498**, 29 (2001).

[21] G. Wilk and Z. Włodarczyk, Phys. Rev. Lett. **84**, 2770 (2000); similar to ‘power-law’ distribution [18].

[22] In the context of velocity/temperature fluctuations this quantity measures  $\overline{(\beta_1 - \beta_0)(\beta_2 - \beta_0)}/\beta_0^2$ , the relative covariance of velocity/temperature fluctuations.

[23]  $\nu \equiv (N_{part}/2)^{1/3} \simeq 5.5(N/N_0)^{1/3}$  for Au ( $N_{part}$  is participant number) [12] estimates mean participant path length in number of encountered nucleons.

[24] Rescaling by  $\mathcal{S}\bar{N}$  is motivated by comparison to a model of A-A collisions as superpositions of independent p-p collisions, in which case the rescaled correlation amplitudes would be independent of centrality.

[25] Total systematic errors for extrapolated quantities in Fig. 4 are due mainly to systematic uncertainty in the data (7-12%) plus uncertainties in correcting for backgrounds and tracking inefficiency (8%) and vary from 11-14% when added in quadrature.

[26] J. Adams *et al.*, Phys. Rev. Lett. **91**, 172302 (2003).